gG and aR fuse DC arcing model for converter sizing

F Reymond-Laruina, Nathalie Barnel, Djamel Hadbi, Philippe Egrot, Loïc Quéval, Marc Petit

gG and aR fuse DC arcing model for converter sizing

F. Reymond-Laruina, N.Barnel, D. Hadbi, P. Egrot, L. Queval and M. Petit,
EDF R&D / GeePs, CentraleSupélec, Sorbonne Uniservité
Avenue des Renardières / 3 Rue Joliot Curie
77250 Moret-sur-Loing, France / 91190 Gif-sur-Yvette, France
E-Mail: frederic.reymond-laruina@edf.fr
URL: https://www.edf.fr / https://www.geeps.centralesupelec.fr

Keywords

«Short circuit», «LVDC», «Protection device», «Modelling», «AC-DC converter».

Abstract

The sizing of AC/DC converter in the context of LVDC distribution grid represents a new challenge. This paper suggests a DC arcing model based on measurements to determine gG and aR fuses behavior, and it is applied to the sizing of a two-level voltage source converter (2L-VSC).

Introduction

Over the past few decades, the development of distributed electricity generation and energy storage systems, as well as the increase in the number of native Direct Current (DC) consumers, have led to an increasing focus on Low Voltage Direct Current (LVDC) distribution grids or at least dedicated DC feeders. Such grids would allow better interaction between applications [1], but also, and more importantly, greater efficiency. First, because the resistance of a DC cable could be lower than that of an AC cable. Second, voltages up to 1500 V are a possibility, resulting in lower losses [2]. Finally, a DC distribution system would centralize and standardize the AC/DC conversion, which is currently performed at the level of each asset. However, possibilities like a full electronic transformer on the substation secondary would not be relevant, due to its cost, size, and higher losses. In this context, the preferred solution is to implement a centralized AC/DC converter on the secondary side on the existing MV/LV transformer to connect a limited number of DC feeders [3].
Despite a large number of commercially available converters, electrical safety remains an obstacle to the deployment of this solution. Indeed, the behavior of a DC short circuit is very different from that of an AC short circuit, due to the presence of capacitors on the DC link and the limited overcurrent tolerance of converter semiconductors. In the event of a fault, these capacitors discharge almost instantaneously, before the grid current feeds the fault by flowing through the converter [4]. Besides, the absence of zero-crossing of the current requires the generation of an opposite voltage to force the decrease of the DC current and interrupt the fault [5]. Several circuit breakers can be found in the literature, such as hybrid or electronic circuit breakers [6], which can achieve response times of 2 ms to 0.1 ms. However, due to their high cost and losses in no fault condition, distribution grid operators might prefer to use fuses because of their simplicity, maturity, and lower cost.

If located on the AC side of the converter, fuses require to oversize the converter [7] to withstand the fault current. If located on the DC side, this constraint can be relieved, thanks to the capacitor discharge which speeds up the fuse blowing. From this idea, a fuse-based strategy has been evaluated in [8] and completed in [9]. Although promising, this solution requires to strongly oversize the capacitor to avoid the voltage reversal of the DC-link. Moreover, the authors don't consider the fuse cutting phase in which the current is still flowing through the converter and can potentially damage it.

This paper proposes to address this issue. First by detailing the fuse features and reviewing existing fuse models. Then by presenting the tests that we performed to get fuse data. Based on this, a modelling of aR and gG fuses is proposed, as well as a generalization of the latter for other test values. Finally, results are applied to a case study and analyzed.

Fuse characteristics and modeling

Fuse protection in distribution grid

A fuse element is made from a high conductivity material with a number of reduced sections commonly called "necks" or "weak spots" (Figure 1). In steady state, at nominal current, the conductive element is at the thermal balance, generating few losses. During overcurrent, thermal balance is breached at the necks level where the current density is higher, eventually leading to the melt of the conductive section. This results in one

or more arcs, depending on the type of fuse element. The arc energy is absorbed by an arc-quenching material surrounding the fuse element, usually graded quartz sand, eventually opening the circuit. The fuse body, composed of an insulated material as ceramic or engineered plastic, contains the quartz arc-quenching material.

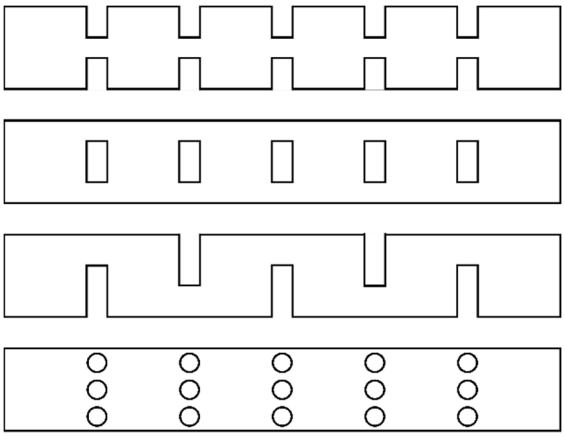

Figure 1 : Typical fuse elements

Fuses are categorized by IEC 60269 by a two-letter code. The first letter defines the function class:

- a: Partial range protection (only short-circuit)
- g: Full range protection (short-circuit and overcurrent)

The second letter correspond to the device protected:

- G: Cable and line protection
- M: Switching device protection in motor circuits
- R: Semiconductor protection
- B: Mine equipment protection
- Tr: Transformer protection
- PV: Photovoltaic protection

aR and gR fuses, often referred as “high-speed”, “ultra-fast” or “semiconductor” fuses, are dedicated to power electronics converter and DC applications with a minimized thermal stress, peak current and arc voltage [10]-[12]. On the other hand, existing AC distribution grids use gG fuses whose requirements are described in [13]. Both technologies may be suitable for LVDC distribution grid. Figure 2 and Figure 3 show a cutting of both technology before and after a blowing: the shape of the fuse element is different as well as the sand compactness.

Figure 2 : Cutting of a new (left) and a blown (right) gG fuse.

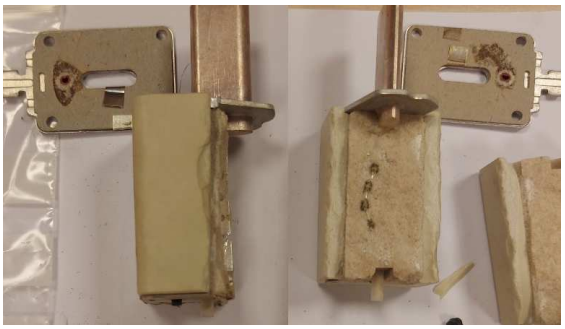

Figure 3 : Cutting of a new (left) and a blown (right) aR fuse.

Existing fuse models

From the previous description, a fuse operates in two phases.

The first phase is called “pre-arcing” and corresponds to the period from the starting of the fault to the fuse element melting. This step is usually modeled by manufacturers as a thermal stress constant, whose expression is given by:

$$I^2 t_{pre-arcing} = \int_0^{t_{pre-arcing}} i_{fuse}^2(t)\, dt \qquad (1)$$

Where $I^2 t_{pre-arcing}$ is the thermal stress [A^2.s], $t_{pre-arcing}$ the pre-arcing time [s] and i_{fuse} the current flowing through the fuse [A].

In the literature, provided the prospective steady state fault current is higher than 7 times the nominal current [14]–[16] and the system time constant is less than 5 ms [15], [17], the fuse operation can be considered adiabatic: there is no heat exchange with the environment allowing to keep constant the thermal stress value. Otherwise, the thermal diffusion inside the fuse must be considered. Several papers address this issue [14]–[16]. Considering parameters of a typical distribution cable and voltage, both conditions on minimal current and system dynamic are met to have an adiabatic behavior of the fuses [8], [9].

The second phase is called “arcing” and

corresponds to the period from the fuse element melting to the arc extinguishing. In [18] a thermo-electrical model, taking into account the geometry of the fuse and its composition, is developed, requiring a lot of information and making it difficult to use for non-manufacturers. In [14] and [19], a simpler electrical model of the fuse arcing as a serial resistor R and capacitor C is provided, but no value is given for these parameters. In addition, this model focuses only on "semiconductor" fuses and considers the voltage rising as instantaneous, which is partially wrong for higher voltage. Reference [20] provides a numerical implementation of this RC fuse model, considering repeated small fault current, but without providing fuse parameters and without considering the thermal behavior. As regards [21], it proposes to identify the R and C parameters by testing "semiconductor" fuses with alternative current and approximating the decreasing current as an RC circuit. This parameters identification is however only performed on simulation.

Proposed fuse modelling method

Based on the previous literature analysis, the main issue is the modelling of the fuse arcing phase. Modelling fuses as a RC circuit seems the most promising option. Therefore, we implement the following steps to model gG and aR fuses:

1. Fuse test campaign
2. Identification of R and C parameters
3. Retrieve a general relation for R and C

The first step aims to provide data on gG and aR fuses. Then for every fuse test, R and C parameters will be retrieve. Considering fuse natural dispersion, differences between identified parameters must appear, despite test parameters are unchanged. To overcome this difficulty, the last step aims to offer a relation to express the average fuse behavior as a function of circuit parameters.

Step 1: Fuse tests

Because existing fuse arcing models focus only on the "semiconductor" fuse, we carried out a fuse testing campaign at the Power Grid Lab in the 50 kA hall, using a high current rectifier (Figure 4). A detailed description of the campaign is available in [22], as well as an analysis of their suitability for a DC distribution application.

Test parameters are $R_{test} = \{0.25, 0.33, 1\}\ \Omega$ and $L_{test} = \{0, 95, 414, 971, 4014\}$ µH with $V_{DC} =$ 490 V, the average value of the rectified AC voltage. In theory, these parameters allow to meet the requirement to get an adiabatic operation of the fuses. The used gG fuse reference is 60320063, by Socomec, while the used aR fuse reference is NH1UD69V63PV, by Mersen. Both are rated for 63 A and 690 V RMS.

In Figure 4, with S_1 opened, there is initially a 55 A current in the fuse, before tripping the fault when closing S_1. For every $\{R_{test}, L_{test}\}$ combination, 5 to 10 fuses were blown up, depending on the variation observed on the total cutting time. The aim is to have a standard deviation less than 10%. Because gG fuses are cheap, supplementary measurements have been performed with two fuses in series. The aim was to try to decrease the cutting time.

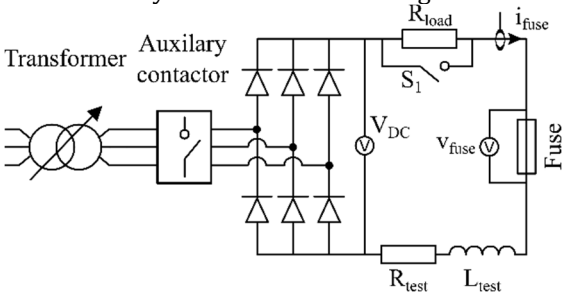

Figure 4 : Schematic of the fuse testing

Preliminary tests without fuses have shown that there is a parasitic inductance due to the transformer and the loop made by the cables. This parasitic inductance L_{par} is about 80 µH and must be added to L_{test}. However, the diode overlapping effect due to this parasitic inductance can be neglected: it last less than 0.3 ms and has no visible influence on the DC voltage. Similarly, the parasitic resistance can be neglected in front of R_{test}.

Some typical current and voltage curves obtained from this test campaign are shown in Figure 5 and Figure 6.

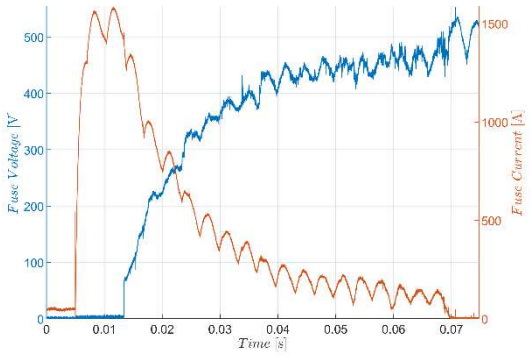

Figure 5 : gG fuse current (right) and voltage (left) during a fault for $R_{test} = 0.33\ \Omega$ and $L_{test} = 95\ \mu H$

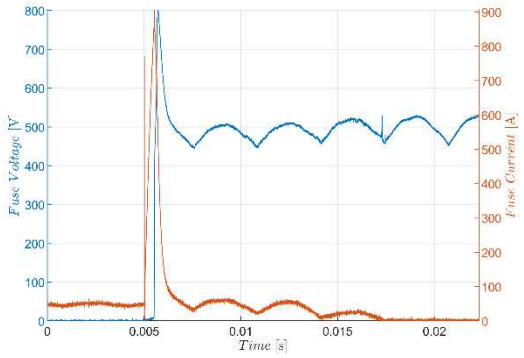

Figure 6 : aR fuse current (right) and voltage (left) during a fault for $R_{test} = 0.33\ \Omega$ and $L_{test} = 95\ \mu H$

Step 2: Retrieving R and C parameters

gG fuse parameters identification

Based on Figure 4, an electrical equivalent circuit is provided in Figure 7. As in [14], fuses are modeled as a serial resistor R and capacitor C, allowing to write equation (2),(3) and (4). Note that an adiabatic behavior is assumed considering prospective fault current.

$$V_{DC} = L_{eq} C \frac{dv_C}{dt^2} + (R_{test} + R)C \frac{dv_C}{dt} + v_C \quad (2)$$

$$i_{fuse}(t) = C \frac{dv_C}{dt} \quad (3)$$

$$v_{fuse}(t) = v_C(t) + R.i_{fuse}(t) \quad (4)$$

where v_C is the voltage across the fuse equivalent capacitor and $L_{eq} = L_{test} + L_{par}$.

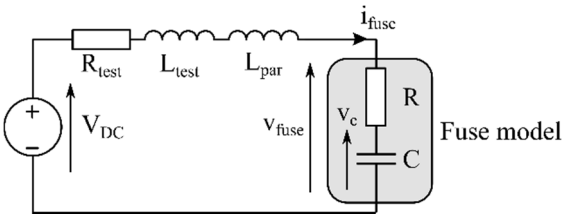

Figure 7 : Equivalent electrical model of the rectifier DC side

Assuming that $\left((R_{test} + R)C\right)^2 - 4L_{eq}C > 0$ and that the fuse current at the beginning of the arc is i_0, the fuse voltage and current are respectively provided by

$$i_{fuse}(t) = A.e^{-\lambda_1 t} + B.e^{-\lambda_2 t} \quad (5)$$

$$v_{fuse}(t) = -A(\lambda_1 L_{eq} + R_{test}).e^{-\lambda_1 t} - B(\lambda_2 L_{eq} + R_{test}).e^{-\lambda_2 t} + V_{DC} \quad (6)$$

Where

- $A = \frac{V_{DC} - i_0(\lambda_2 L_{eq} + R_{test})}{L_{eq}(\lambda_1 - \lambda_2)}$
- $B = \frac{V_{DC} - i_0(\lambda_1 L_{eq} + R_{test})}{L_{eq}(\lambda_2 - \lambda_1)}$
- $\lambda_1 = \frac{-(R_{test}+R)C + \sqrt{((R_{test}+R)C)^2 - 4L_{eq}C}}{2}$
- $\lambda_2 = \frac{-(R_{test}+R)C - \sqrt{((R_{test}+R)C)^2 - 4L_{eq}C}}{2}$

The non-linear least squares formulation, as described by (7), is used on the measured current and voltage. Fitting the theoretical curve with the experimental result is performed with the Levenberg-Marquardt algorithm. Results are shown in red in Figure 8 to Figure 11. This formulation allows to converge to the same parameters value for current and voltage.

$$\min\Big(\big(i_{fuse}(t,R,C) - i_{fuse,meas}\big)^2 + \big(v_{fuse}(t,R,C) - v_{fuse,meas}\big)^2\Big) \quad (7)$$

Where $i_{fuse,meas}$ and $v_{fuse,meas}$ are respectively the measured current and voltage in the fuse during the test campaign.

It must be noted that Figure 10 and Figure 11 corresponds to two gG fuses in series, meaning that two fuses can have a similar behavior to a single one and can be represented according to the same model, but with different parameters.

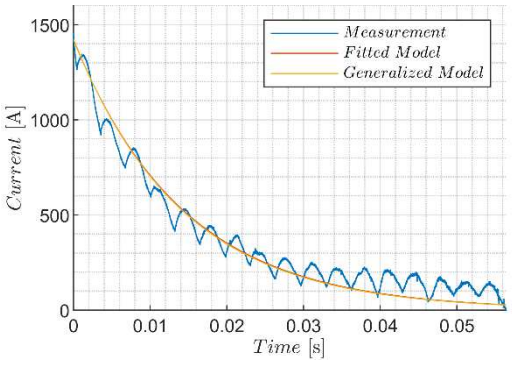

Figure 8 : gG fuse current during arcing for $R_{test} = 0.33\ \Omega$ and $L_{test} = 95\ \mu H$, with measurement (bleu), fitted model (red) and generalized model (yellow)

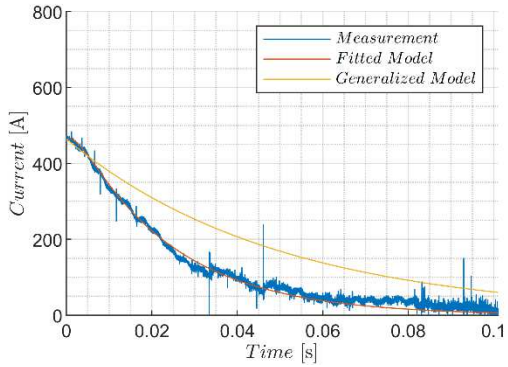

Figure 9 : Serial gG fuse current during arcing for $R_{test} = 1\,\Omega$ and $L_{test} = 4010\,\mu H$, with measurement (bleu), fitted model (red) and generalized model (yellow)

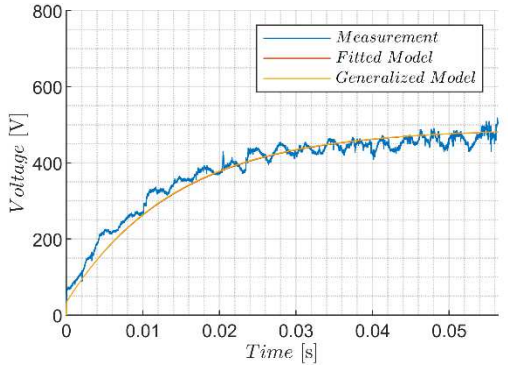

Figure 10 : gG fuse voltage during arcing for $R_{test} = 0.33\,\Omega$ and $L_{test} = 95\,\mu H$, with measurement (bleu), fitted model (red) and generalized model (yellow)

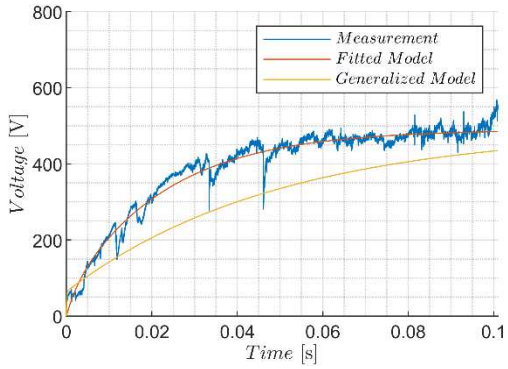

Figure 11 : Serial gG fuse voltage during arcing for $R_{test} = 1\,\Omega$ and $L_{test} = 4010\,\mu H$, with measurement (bleu), fitted model (red) and generalized model (yellow)

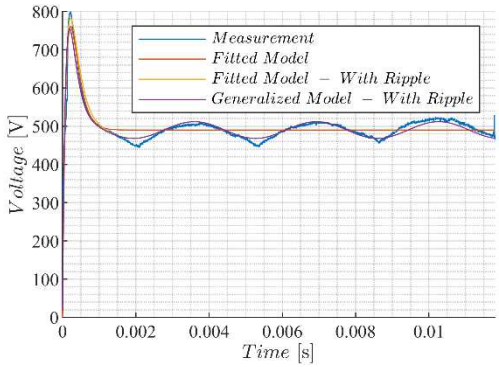

Figure 12 : aR fuse voltage during arcing for $R_{test} = 0.33\,\Omega$ and $L_{test} = 95\,\mu H$, with measurement (bleu), fitted model with and without ripple (red and yellow) and generalized model with ripple (purple)

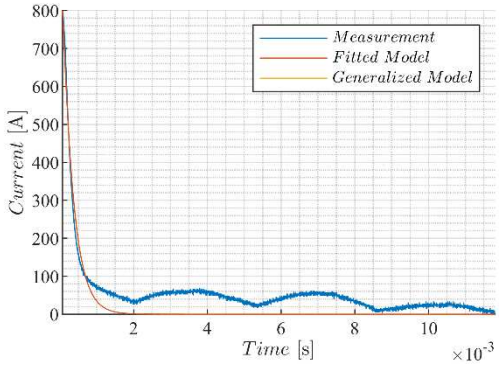

Figure 13 : aR fuse current during arcing for $R_{test} = 0.33\,\Omega$ and $L_{test} = 95\,\mu H$, with measurement (bleu), fitted model (red) and generalized model (yellow)

aR fuse parameters identification

None of the models of the literature has been found to be suitable for modelling the arcing phase in an aR fuse, due to the non-instantaneous voltage rise phase. To overcome this issue, we propose to reuse the previously developed current model and give an analytical model of the voltage with different parameters, leading respectively to equation (5) and (11).

$$v_1(t) = k.V_{DC}\left(1 - e^{-\frac{t}{\tau_1}}\right) \quad (8)$$

$$v_2(t) = (k-1)V_{DC}\left(1 - e^{-\frac{t}{\tau_2}}\right) \quad (9)$$

$$v_{ripp}(t) = A.cos\left(\frac{2\pi}{T}t + \varphi\right) \quad (10)$$

$$v_{fuse}(t) = v_1(t) - v_2(t) + v_{ripp}(t) \quad (11)$$

Where k is a distribution coefficient, (τ_1, τ_2) are time constant [s], A is the amplitude of the voltage

ripple around V_{DC} in steady state [V], T is the period of the rectified voltage [s], approximately 3.3 ms, and φ is the initial phase shift of the voltage.

The parameters of each model are then determined independently, using non-linear least squares formulation, as described by (12) and (13). The Levenberg-Marquardt algorithm is used to solve both problems. The results are shown in Figure 12 and Figure 13 and will be analyzed later.

$$\min\left(\left(i_{fuse}(t,R,C)-i_{fuse,meas}\right)^2\right) \quad (12)$$

$$\min\left(\left(v_{fuse}(t,k,\tau_1,\tau_2)-v_{fuse,meas}\right)^2\right) \quad (13)$$

Step 3: Parameters generalization

Although previous modelling allows an accurate representation of the fuse arcing step, this behavior is described only for specific points. Therefore, we aim to look for generalized models explaining the evolution of the fuse parameters between each test. The R-squared, or R^2, is used as an indicator of the model quality. Comprised between 0 and 1, it describes to what extent a regression model fits the data. In other words, the closer the value is to 1, the better the model explains the variation in the data. Besides, rather than using non-linear least squares method, we are using the least absolute residual (LAR) method, which aims to make the fit incentive to outlying data points, by using the absolute difference of the residuals, rather than the squared differences.

With reference to equations (5) and (6), we propose to determine time constant parameters $R_{eq}C$ and $L_{eq}C$, where $R_{eq} = R_{test} + R$. These parameters can be determined respectively by polynomial equations equation (14) and (15). Based on these two equations, we calculate R and C.

$$R_{eq}C = aR_{test}{}^2 + bL_{eq}R_{test} + cR_{test} + dL_{eq} + e \quad (14)$$

$$L_{eq}C = a\frac{L_{eq}}{R_{test}} + bR_{eq}C + c \quad (15)$$

Note that for aR fuse, equations (15) must be replaced by (16) and that these two parameters can only be used to estimate the fuse current.

$$L_{eq}C = a\left(R_{eq}C\right)^2 + b\frac{L_{eq}}{R_{test}}.R_{eq}C + cR_{eq}C + d\frac{L_{eq}}{R_{test}} + e \quad (16)$$

Table 1 gives the parameters of each equation depending on the fuse type and on the assembly, as well as the R^2 value of each equation.

Table 1: Coefficient to use to for equations(14) (15) (16), depending on the assembly and the fuse type

Fuse		gG		aR
Assembly		Alone ($\times 10^{-3}$)	Series ($\times 10^{-3}$)	Alone ($\times 10^{-3}$)
$R_{eq}C$ [s]	a	19.69	53.08	0.1212
	b	-0.8952	-0.7066	-0.3708
	c	19.71	-12.35	0.2296
	d	2.109	1.327	0.7602
	e	5.143	5.508	0.09666
	R^2	0.996	0.978	0.984
$L_{eq}C$ [s]	a	1.009	1.378	104.6
	b	-1.234	5.6	0.1019
	c	-0.3031	-0.4689	0.1633
	d			-8.45×10^{-5}
	e			5.52×10^{-5}
	R^2	0.878	0.844	0.986

For the aR fuse voltage, the parameters (τ_1, τ_2) can be determined using equation (17) while parameter k require using (18).

$$\tau_{1,2} = a\frac{L_{eq}}{R_{test}} + bR_{eq}C + c \quad (17)$$

$$k = a\left(\frac{L_{eq}}{R_{test}}\right)^2 + b\frac{L_{eq}}{R_{test}}.R_{eq}C + c\frac{L_{eq}}{R_{test}} + dR_{eq}C + e \quad (18)$$

Table 2 gives the parameters of each equation, to determine the aR fuse voltage during arcing.

Table 2: Coefficient to use to determine aR fuse voltage parameters

	τ_1	τ_2	k
a	1.339×10^{-5}	1.397×10^{-5}	-2.958
b	0.4401	0.4402	-7343
c	-5.152×10^{-6}	-5.171×10^{-6}	30.11
d			-3233
e			865.3
R^2	0.945	0.945	0.926

Note that for using equation (14)-(18), L_{eq} is express in mH, and consequently $\frac{L_{eq}}{R_{test}}$ is in ms. Other variables $R_{eq}C, L_{eq}C, R_{test}, R_{eq}, \tau_1, \tau_2, k$ are expressed in international units.

Analysis of results

The presented RC generalized modeling allows to describe accurately current in gG and aR fuses, as shown in Figure 8, Figure 9 and Figure 13.

Nonetheless, this result must be nuanced in the case of aR fuses, because if the initial current decreasing is well-modeled, the arc ending doesn't fit the measurement, as illustrated in Figure 13 : the current converges to zero faster than the measurement. This behavior deviation must urge us to take a safety factor of at least 5, when estimating the fuse arcing time with this model. As regards using this model for thermal stress estimation, the safety factor can be neglected insofar as the current not modelled is small and therefore hasn't a significant influence on the fuse overall thermal stress. Focusing only on the arcing step, the underestimation of the thermal stress is around 15%.

Regarding voltage estimation, two models have been proposed. While aR fuse voltage model allows to consider the grid voltage ripple, it can only be estimated analytically. An underestimation of 5% can be noted on the peak voltage with the generalized model, while the fitted model underestimation value is only 2.5%. One the other hand, the gG fuse voltage model considers the initial voltage jump, but not the voltage ripple, being an analytical model. Implementation of R and C parameters with a simulated rectifier can solve this issue. This perspective allows us to highlight the main advantage of the gG fuse model: it can be implemented in a simulation to get current and voltage at the same time.

Despite all these promising results, a deviation can be noted in Figure 9 and Figure 11, between the measured values and the generalized ones. The deviation originates from the natural deviation between the fuses. By plotting more measurement, as in Figure 14, it appears that the generalized model is still valid. The proposed work estimates an average behavior and doesn't consider extreme situations. This behavior also explains the underestimation of the voltage peak in Figure 12.

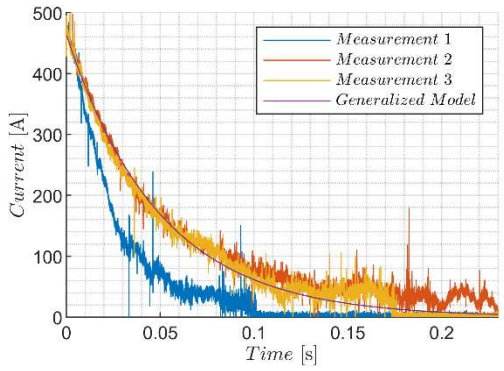

Figure 14 : Serial gG fuse current during arcing for $R_{test} = 1\,\Omega$ and $L_{test} = 4010\,\mu H$ with 3 different measurement (blue, red and yellow) and the generalized model (purple)

Application & Limitations

Implementation of the model in simulations

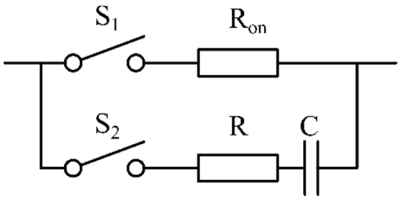

Figure 15 : Equivalent model of a fuse

The equivalent model of a fuse is provided in Figure 15. In steady state the fuse is a resistance R_{on} whose value in given by the manufacturer's datasheet. During the pre-arcing phase, this model can be kept, though some authors underlines that the resistance varies with the current [1], [2]. On the Figure 15, S_1 is closed and S_2 is open.

The pre-arcing phase ends when (19) is not verified anymore. S_1 switches off and S_2 switches on.

$$I^2 t_{pre-arcing} \geq \int_{t_{start}}^{t} i_{fuse}^2(u)\,du \qquad (19)$$

Where $I^2 t_{pre-arcing}$ is the fuse thermal stress according to the datasheet [A^2.s], t_{start} the short-circuit starting instant [s], t the current instant [s] and i_{fuse} the current flowing through the fuse [A].

For the arcing phase, the R and C parameters of the model can be determined directly from equations (14),(15) and (16), depending on the fuse technology.

Application example

To illustrate the use of the fuse model, we consider a two-level voltage source converter (2L-VSC) feeding a resistive load through cable. The parameters of the system are provided in Table 3.

Table 3 : AC and DC grid parameters

Transformer	
Primary voltage	20 kV
Secondary voltage	400 V
Short-circuit voltage	4 %
DC Cable	
Linear inductance	0,071 Ω/km
Linear resistance	0,124 Ω/km
Length	600 m
Fault	

Location l_{fault}	150 m
Impedance	1 mΩ
Resistive Load	
Power	20 kW
Converter	
Interface Inductance	1.5 mH
Capacitor	4500 µH

In the case of a 2L-VSC, the behaviour of the converter in the event of a fault must be compared with that of a rectifier studied previously. First, using equations (20) and (21), the equivalent DC resistance and inductance must be determined. In these equations, $L_{eq,DC}$ and $R_{eq,DC}$ correspond respectively to the equivalent DC inductance and resistance, including the cables and loop inductance. $L_{eq,AC}$ and $R_{eq,AC}$ describes respectively the equivalent DC inductance and resistance of the AC filter and insulation transformer if used. Finally, using equations (14),(15) and (16), the R and C parameters can be determined.

$$L_{eq} = L_{eq,DC} + \frac{3}{2} L_{eq,AC} \quad (20)$$

$$R_{eq} = R_{eq,DC} + \frac{3}{2} R_{eq,AC} \quad (21)$$

This method has been used for the 2L-VSC described in [7], with and without control. This last point corresponding to a rectifier with a high interface inductance on the AC grid and no DC-link capacitors. Figure 16 shows the resulting thermal stress of each diode during a pole-to-pole fault is this case. Meanwhile Figure 17 shows the results for a 2L-VSC. These figures highlight the necessity for the converter diodes to withstand at least a thermal stress of 6000 A^2s in passive diode rectifier and only 4500 A^2s with active rectifier. The capacitor discharge allowing to decrease sharply the pre-arcing time. This analysis must be completed by repeating this process for different fault inception time and location, in order to get the most critical case, which is not known in advance.

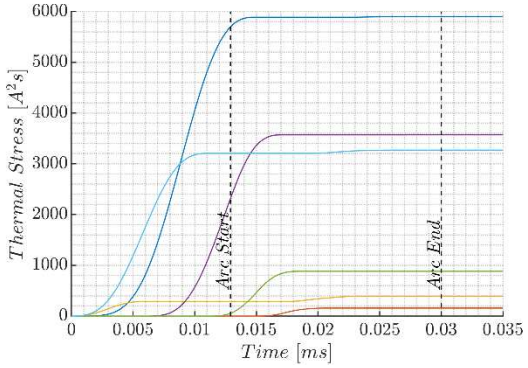

Figure 16 : Rectifier diodes thermal stress during a pole-to-pole fault, located at 150 m, and with a 1.5 mH AC. Beginning and ending time of the gG fuse arc are indicated with dashed black line.

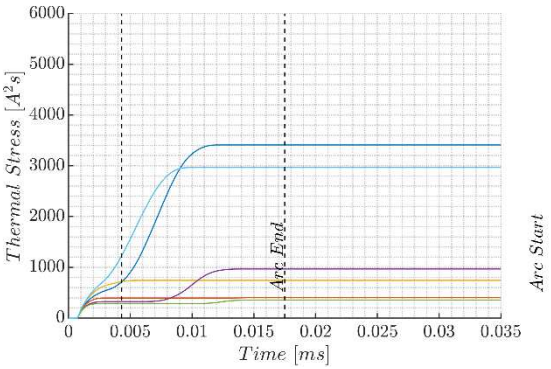

Figure 17 : 2L-VSC diodes thermal stress during a pole-to-pole fault, located at 150 m, and with a 1.5 mH AC. Beginning and ending time of the gG fuse arc are indicated with dashed black line.

Compared to manufacturer methods, our sizing method allows to decrease the oversizing of the converter. Indeed, manufacturers recommend choosing a fuse with a thermal stress 20% lower than that of the converter diode. Knowing that gG fuses have a thermal stress of 28,000 A^2s, this would be equivalent to choosing diodes with a thermal stress of 35,000 A^2s. Alternatively, faster fuses could have been used. The studied aR fuses could meet the manufacturer requirement, however they are far more expensive than classical gG fuses. They cost roughly 230€ per unit, whereas gG fuses cost only 4€ per unit.

Model limitations

It must be noted that the fuse arcing time is faster than the one observed on the rectifier, despite having the same RL value. One explanation is the DC-link capacitors absorb some of the current as the voltage rises and the circuit opens. Another reason could be the effect of the tie reactors which limit the voltage applied during the fault. Both reasons must encourage us to perform new tests to quantify the response of fuses when a capacitor is inserted. Similar tests must be performed to determine if the fuses have the same behavior with a DC voltage lower than the one of a rectifier and validate the impact of the tie reactor on the fuse R and C parameters.

As it stands, the fuse model we achieved is only valid for three-phase diode rectifiers. Tests must also be added to approximate a clean fault case, where the resistance on the DC bus is almost zero. Depending on the input, some values provided by

equations (14),(15) and (16) are not physical (ie a negative resistance).

Conclusion

In this paper, a model for gG and aR fuse has been implemented and validated. For gG fuses, the proposed RC model can be implemented in simulation to determine the fuse current and voltage, while for aR fuses only the current is relevant. An analytical model for the voltage is proposed as a substitute. The large number of fuses tests allowed us to propose and validate a method of generalization to determine the fuse response for different type of RL circuit. This method has been implemented for a 2L-VSC and allowed to highlight the necessity to perform more fuse testing to consider the participation of the DC-link capacitor in the fuse response, which tends to accelerate the fault interruption.

References

[1] J. J. Justo, F. Mwasilu, J. Lee, and J.-W. Jung, 'AC-microgrids versus DC-microgrids with distributed energy resources: A review', *Renewable and Sustainable Energy Reviews*, vol. 24, 2013

[2] K. Smith, D. Wang, A. Emhemed, S. Galloway, and G. Burt, 'Overview paper on: low voltage direct current (LVDC) distribution system standards', p. 24.

[3] J. E. Huber and J. W. Kolar, 'Applicability of Solid-State Transformers in Today's and Future Distribution Grids', *IEEE Trans. On Smart Grid*, vol. 10, 2019.

[4] S.-M. Xue and C. Liu, 'Line-to-Line Fault Analysis and Location in a VSC-Based Low-Voltage DC Distribution Network', *Energies*, vol. 11, 2018

[5] Y. Pelenc, 'Interruption des circuits alimentés en courant continu', *Techniques de l'Ingénieur*, 2002

[6] R. Rodrigues, Y. Du, A. Antoniazzi, and P. Cairoli, 'A Review of Solid-State Circuit Breakers', *IEEE Trans. Power Electronic*, vol. 36, 2021

[7] F. Reymond-Laruina, L. Quéval, D. Hadbi, P. Egrot, M. Cordonnier, and S. Mercier, 'Impacts of low voltage distribution grid resilience constraints on AC/DC converter sizing', 27th International Conference on Electricity Distribution, Rome, Italy, 2023

[8] S. Ravyts, G. V. den Broeck, L. Hallemans, M. D. Vecchia, and J. Driesen, 'Fuse-Based Short-Circuit Protection of Converter Controlled Low-Voltage DC Grids', *IEEE Trans. Power Electron.*, vol. 35, 2020

[9] S.-Y. Lee, Y. Son, H.-J. Cho, and S.-K. Sul AE, 'Normalization of Capacitor-Discharge I^2t by Short-Circuit Fault in VSC-based DC System', *IEEE Trans. Power Electron.*, 2021

[10] 'Fusible Overcurrent Protection for DC Applications', EATON, Technical Report, 2020

[11] 'Fuse Systems Configuration Manual 2012', Siemens, Technical Report, 2012

[12] 'Protecting semiconductors with high-speed fuses', Bussman Series, Technical Report, 2016

[13] Jean-Philippe SIGAL, 'Protection du réseau BT contre les courts-circuits', ERDF, Technical Report, 2014

[14] T. Tanaka and M. Yamasaki, 'Modeling of fuses for melting time and fusing current analysis', *10th International Workshop on Computational Electronics*, Chicago, USA, 2004

[15] S. S. Memiaghe, 'Modélisation du régime de préarc dans les fusibles', Université Blaise Pascal - Clermont-Ferrand II, 2010

[16] S.-Y. Lee *et al.*, 'Simplified Thermal Model of Semiconductor Fuse for DC Distribution System', *10th International Conference on Power Electronics and ECCE Asia*, Busan, South Korea, 2019

[17] 'IEEE Guide for the Protection of Stationary Battery Systems', IEEE, 2012

[18] X. Just, 'Interaction entre arc et matière granulaire lors d'une coupure ultra-rapide dans un fusible', Université Grenoble Alpes, 2016

[19] T. Tanaka, H. Kawaguchi, T. Terao, T. Babasaki, and M. Yamasaki, 'Modeling of fuses for DC power supply systems including arcing time analysis', *29th International Telecommunications Energy Conference*, Rome, Italy, 2007

[20] D. Li and L. Qi, 'Energy based fuse modeling and simulation', *IEEE Electric Ship Technologies Symposium*, Arlington, USA, 2013

[21] J. J. Deroualle, 'Modeling of High-Speed Fuses for Selectivity Study in DC Shipboard Power System', *IEEE Fourth International Conference on DC Microgrids*, Arlington, USA, 2021

[22] D. Hadbi, L. C. Delgado, and F. Reymond-Laruina, 'DC short-circuit behaviour of LVAC fuses', 27th International Conference on Electricity Distribution, Rome, Italy, 2023